Available online at www.sciencedirect.com
ScienceDirect
Tetrahedron 63 (2007) 10731–10742
Tetrahedron

1,3-Alternate calix[4]arene nitronyl nitroxide tetraradical and diradical: synthesis, X-ray crystallography, paramagnetic NMR spectroscopy, EPR spectroscopy, and magnetic studies

Andrzej Rajca,[a,*] Maren Pink,[b] Sumit Mukherjee,[a] Suchada Rajca[a] and Kausik Das[a]

[a]*Department of Chemistry, University of Nebraska, Lincoln, NE 68588-0304, USA*
[b]*Department of Chemistry, Indiana University, Bloomington, IN 47405-7102, USA*

Received 5 May 2007; revised 3 July 2007; accepted 5 July 2007
Available online 25 July 2007

Abstract—Calix[4]arenes constrained to 1,3-alternate conformation and functionalized at the upper rim with four and two nitronyl nitroxides have been synthesized, and characterized by X-ray crystallography, magnetic resonance (EPR and ^{1}H NMR) spectroscopy, and magnetic studies. Such calix[4]arene tetraradicals and diradicals provide scaffolds for through-bond and through-space intramolecular exchange couplings.

1. Introduction

Macrocycles based upon calix[4]arenes have been utilized as effective frameworks for high-spin polyradicals.[1–4] In such macrocycles, four triphenylmethyl radicals are connected in-chain, forming cyclic cross-conjugated π-systems, in which the radicals are coupled through *m*-phenylene, a well-known, robust through-bond ferromagnetic exchange coupler (Fig. 1).[5–11]

The tetraradical possesses a high-spin quintet (S=2) ground state, with a large energy gap separating the S=2 ground state from the S<2 excited states.[12] The polyarylmethyl calix[4]arene S=2 tetraradical (Fig. 1) is the key building block for the bottom-up, modular design of high-spin organic polyradicals.[1–4,13–19] Examples of such polyradicals include organic molecules with the highest values of the total spin quantum number up to S=13 and the first organic polymer with magnetic ordering (magnetic ordering temperature of about 10 K).[16,17]

Recently, calix[4]arene and resorcinarene macrocycles have been adopted as scaffolds for attaching two or four organic radicals as pendants at the upper or lower rim.[20–24] For example, direct attachment of radicals at the upper rim of calix[4]arenes that are constrained to an 1,3-alternate or cone conformation has provided unique models for the dissection

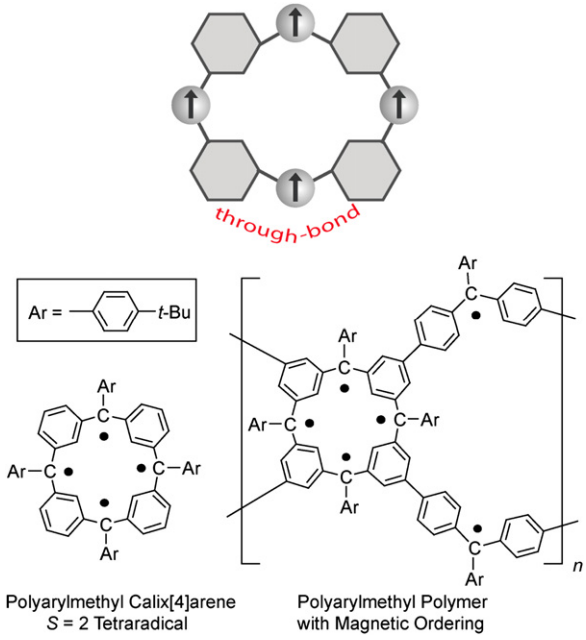

Figure 1. Calix[4]arenes functionalized with in-chain radicals forming a cross-conjugated π-system: polyarylmethyl S=2 tetraradical and polymer with magnetic ordering.

of the through-bond and through-space intramolecular exchange coupling, as well as for the study of conformational dependence of through-bond coupling (Fig. 2).[23,24] The through-bond coupling between the adjacent radicals is mediated by the relatively extended radical–*m*-phenylene–

Keywords: Calixarene; Nitroxide; Diradical; Tetraradical; Magnetic properties; Paramagnetic NMR spectroscopy.
* Corresponding author. Tel.: +1 402 472 9196; fax: +1 402 472 9402; e-mail: arajca1@unl.edu

0040–4020/$ - see front matter © 2007 Elsevier Ltd. All rights reserved.
doi:10.1016/j.tet.2007.07.051

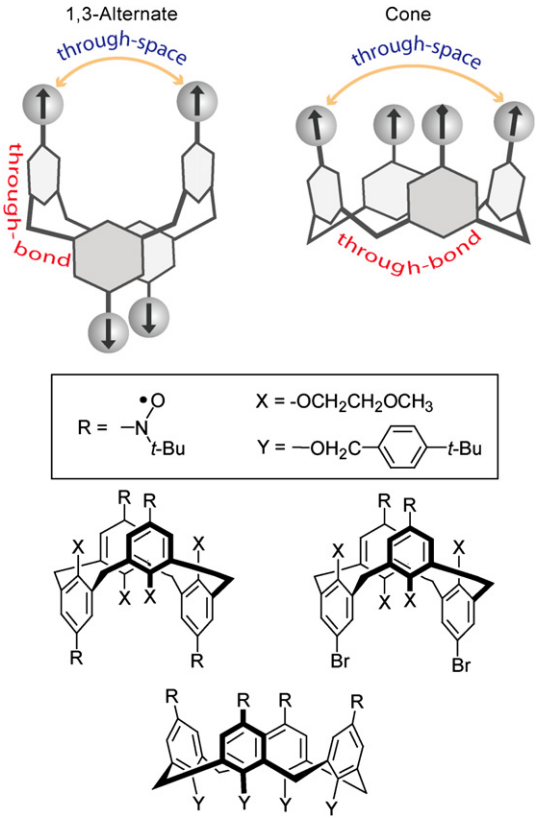

Figure 2. Calix[4]arenes functionalized with pendant radicals: 1,3-alternate and cone calix[4]arene scaffolds with two or four nitroxide radicals.

CH_2–*m*-phenylene–radical coupling pathway, and through-space coupling is found between the diagonal radicals.

Magnetic studies of ambient stable nitroxide tetraradicals (Fig. 2) indicate that the through-bond exchange coupling, mediated by the nitroxide–*m*-phenylene–CH_2–*m*-phenylene–nitroxide exchange coupling pathway, is antiferromagnetic in the 1,3-alternate conformation, while the exchange coupling is ferromagnetic in the cone conformation.[24] Through-space nitroxide–nitroxide exchange couplings are antiferromagnetic in both cone and 1,3-alternate calix[4]arene tetraradical, as well as in the 1,3-alternate calix[4]arene diradical. X-ray structures of the diradical and tetraradical reveal N···N distances of 5–6 Å between the diagonal nitroxides. Both through-bond and through-space exchange couplings are on the order of 1 K, i.e., $|J/k| \approx 1$ K.[24]

The radical functionalized 1,3-alternate calix[4]arene is an attractive model system with well-defined radical–radical interactions, such as exchange coupling and magnetic dipole–dipole coupling, for probing the dependence of electron spin relaxation on the strength of radical–radical interactions. Recently, the 1,3-alternate calix[4]arene nitroxide tetraradical and diradical were employed as model systems for the study of electron spin relaxation,[25] aimed at the development of functional paramagnetic contrast agents for electron paramagnetic resonance imaging (EPRI) and magnetic resonance imaging (MRI).[26–30] These nitroxide polyradicals provide the probes for well-defined and moderately strong radical–radical interactions.

We have sought model systems, in which we anticipate significantly weaker radical–radical interactions, such as nitronyl nitroxide tetraradical **1** and diradical **2** (Fig. 3).[31,32]

The analysis of the EPR data in the literature indicates that the ^{1}H-hyperfine splittings (a_H) at the *para*- and *ortho*-positions in 2-phenyl-4,4,5,5-tetramethylimidazoline-1-oxyl-3-oxide (phenyl nitronyl nitroxide) monoradical are about 1/5, compared to those in the corresponding nitroxide monoradical.[33,34] Based upon the empirical relationship ($2J/k \sim |a_H|^2$),[2] which reflects the correlation between the strength of through-bond exchange coupling mediated by *m*-phenylene and the delocalization of spin density into the *m*-phenylene, the singlet–triplet gap, $2J/k$, for *m*-phenylene-based nitronyl nitroxide diradicals should be smaller by a factor of 1/25 than that for the corresponding nitroxide diradicals. This estimate is supported by the experimental values of the singlet–triplet gaps in *m*-phenylene-based diradicals that are $2J/k \approx +600$ K and +20 K for bis(nitroxide) and bis(nitronyl nitroxide), respectively.[30,35,36] Therefore, the through-bond exchange coupling mediated by the *m*-phenylene–CH_2–*m*-phenylene unit in nitronyl nitroxide tetraradical **1** is expected to be weaker by a factor of 25–30, compared to $|J/k| \approx 1$ K in the corresponding nitroxide tetraradical.

Through-space radical–radical interactions depend on the radical–radical distance (r), with exponential and $1/r^3$ dependencies for through-space exchange coupling and magnetic dipole–dipole coupling, respectively. Because the 4,4,5,5-tetramethylimidazoline-1-oxyl-3-oxide (nitronyl nitroxide) moieties are more bulky compared to the *tert*-butylnitroxide moieties, the distances between co-facial nitronyl nitroxides in tetraradical **1** and in diradical **2** are expected to be greater than those in the corresponding nitroxide tetraradical and diradical. In addition, the spin density is primarily delocalized over four atoms (N_2O_2) in the nitronyl nitroxide moieties, compared to the delocalization over two atoms (NO) in the nitroxide moieties. These increased radical–radical distances and increased delocalization of spin density should lead to weaker through-space radical–radical interactions between co-facial nitronyl nitroxides in **1** and **2**.

This article describes the synthesis and characterization of ambient stable nitronyl nitroxide tetraradical **1** and diradical **2** in the fixed 1,3-alternate calix[4]arene conformations (Fig. 3).

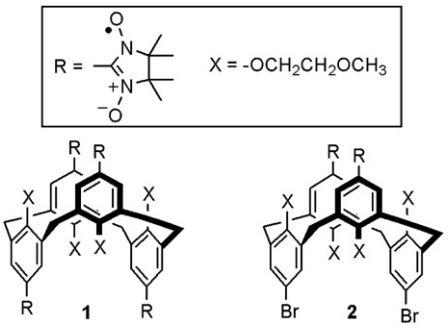

Figure 3. Nitronyl nitroxide tetraradical **1** and diradical **2** with constrained conformations of 1,3-alternate calix[4]arene.

2. Results and discussion

2.1. Synthesis

The synthesis starts from tetrabromocalix[4]arene **3**, constrained in the 1,3-alternate conformation (Scheme 1).[37,24] Li/Br exchange on **3** with an excess amount of *t*-BuLi gives intermediate tetrakis(aryllithium), which is reacted with *N*-methylformanilide, to provide tetraaldehyde **4**.[38]

An analogous procedure, in which the *t*-BuLi is replaced with *n*-BuLi (2 equiv),[24] gives dialdehyde **5**. In the next step, well-stirred suspensions of **4** and **5** in methanol are condensed with 2,3-bis(hydroxyamino)-2,3-dimethylbutane in the presence of *p*-TsOH,[39] to provide tetrakis(1,3-dihydroimidazolidine) **6** and bis(1,3-dihydroimidazolidine) **7**, respectively. Oxidations of **6** and **7** in water/dichloromethane at 0 °C, using 1 equiv of $NaIO_4$ per 1,3-dihydroimidazolidine,[39] give tetraradical **1** and diradical **2** in good yields.

The presence of hydroxyl groups in **6** and **7** is confirmed by IR (e.g., $\nu_{O-H} \approx 3300\ cm^{-1}$) and ^1H NMR (600 MHz, DMSO-d_6) spectra; in particular, D_2O-exchangeable 8-proton or 4-proton singlets at 7.6–7.7 ppm are found in the ^1H NMR spectra. The additional evidence for 1,3-dihydroimidazolidines is provided by the assignment of the methine protons (4-proton and 2-proton singlets at 4.4–4.5 ppm), which are slightly upfield shifted from the typical 4.6–4.8 ppm range; the methyl groups on the imidazolidine rings appear as two singlets at ~1.0 ppm for each compound. ^{13}C NMR (150 MHz, DMSO-d_6) spectra for **6** and **7** show all expected resonances in the aromatic and aliphatic regions, including the resonances for methine carbons of the imidazolidine rings at 89–90 ppm.

2.2. Molecular structure of 1 and 2

Nitronyl nitroxide tetraradical **1**[40] and diradical **2** (Ref. S5, Supplementary data) crystallize with two unique molecules per asymmetric unit and include solvent in the structures. Inefficient packing of the calix[4]arenes leaves voids in the structure. This, together with the inherent flexibility of the methoxyethylene chains and the rotational freedom of the imidazole rings, gives rise to extensive disorder. In fact, the diffraction pattern indicated highly disordered structures by streaks, diffuse (non-Bragg) scattering, and rapidly weakening diffraction at higher (sin θ)/λ values (at medium and high resolution). Consequently, the resulting structures have relatively high *R*-values. However, the standard uncertainties of geometrical parameters are reasonable for **1** and the disorder is affecting solvent molecules, side chains and the imidazoline rings (rotationally disordered about the bond to the calixarene frame) only but not the calixarene core. The displacement parameters (Fig. 4) are acceptable as well. We therefore assert that the X-ray structure of **1** (Fig. 4 and Fig. S1, Supplementary data) provides correct connectivity and reliable geometry, and distances discussed (vide infra) are not adversely affected by the low quality of the entire structure with disorder in side chains and solvent molecules. Moreover with two independent molecules, we have several observations for distances and angles discussed, which fit quite well and are within the expected ranges. However, **2** should be viewed as a preliminary result that confirms the connectivity and overall geometry of the diradical only (Figs. S2 and S3, Supplementary data).

The structure of tetraradical **1** has four pairs of the co-facial nitronyl nitroxide groups (ONCNO), due to the presence of two crystallographically unique molecules. The disorder of two ONCNO groups, with the 50:50 site occupancy in each case, is associated with the rotation of the 4,4,5,5-tetramethylimidazoline-1-oxyl-3-oxide moiety about the CC bond connecting it to the benzene ring. For each aryl nitronyl nitroxide moiety, the ONCNO groups are twisted about this CC bond, forming torsional angles of 10–40° with the benzene rings. In most pairs of co-facial radicals, the ONCNO groups are nearly parallel; the radical–radical distances are rather long, as measured by the C···C distances that are

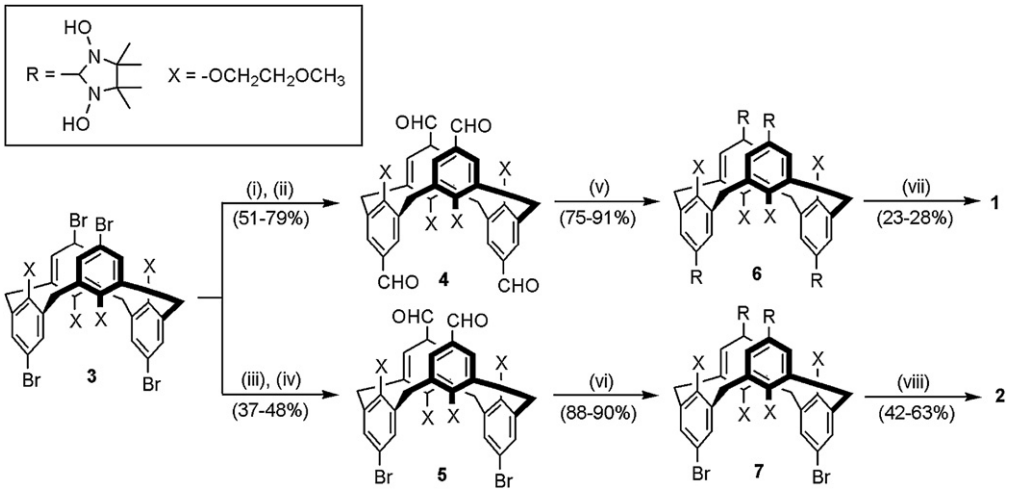

Scheme 1. Synthesis of nitronyl nitroxide tetraradical **1** and diradical **2**. Reagents and conditions: (i) *t*-BuLi (8 equiv), THF, −78 °C for 2 h, then −20 °C for 15 min; (ii) PhN(Me)CHO (4 equiv), −78 °C then slowly warm up to room temperature overnight; (iii) *n*-BuLi (2 equiv), THF, −78 °C for 2 h, then −20 °C for 15 min; (iv) PhN(Me)CHO (2.4 equiv), −78 °C then slowly warm up to room temperature overnight; (v) 2,3-bis(hydroxyamino)-2,3-dimethylbutane (10 equiv), *p*-TsOH (0.2 equiv), MeOH, 60–65 °C for 2–2.5 days; (vi) 2,3-bis(hydroxyamino)-2,3-dimethylbutane (5 equiv), *p*-TsOH (0.2 equiv), MeOH, 55–60 °C for 2–3 days; (vii) $NaIO_4$ (4 equiv), CH_2Cl_2, H_2O, 0 °C; (viii) $NaIO_4$ (2 equiv), CH_2Cl_2, H_2O, 0 °C.

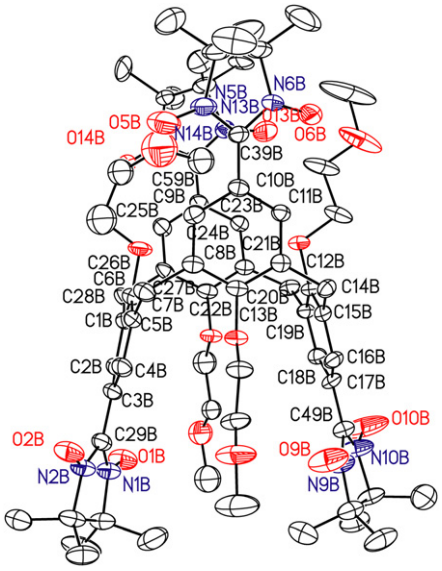

Figure 4. Molecular structure and conformation for nitronyl nitroxide tetraradical **1** with constrained conformation of 1,3-alternate calix[4]arene. Carbon, nitrogen, and oxygen atoms are depicted with thermal ellipsoids and spheres set at the 50% probability level. Only one of the two unique molecules of **1**, omitting disorder, hydrogen atoms, and the solvent of crystallization (benzene and water), is shown.

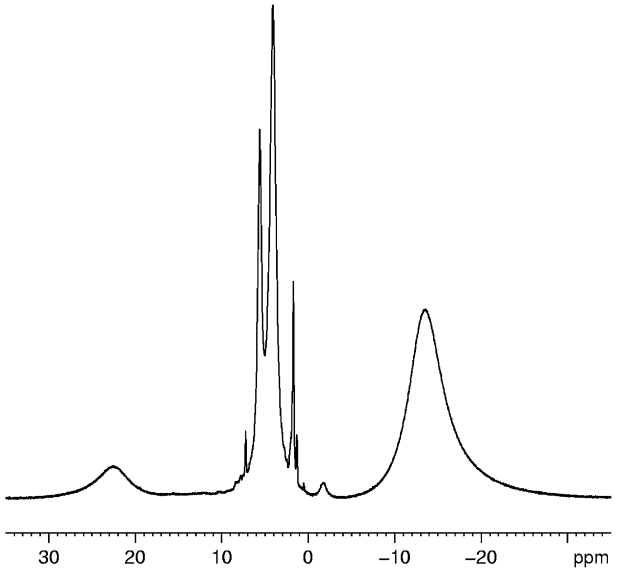

Figure 5. ^{1}H NMR (600 MHz, LB=1 Hz) spectrum for ~70 mM nitronyl nitroxide tetraradical **1** in chloroform-*d*. The weak sharp singlet at 7.26 ppm and broad singlet at −1.7 ppm correspond to the residual non-deuterated chloroform and water peaks. The chemical shift (+1 to −2 ppm) and integration of the broad singlet are sample (concentration) dependent. The other sharp, relatively weak peaks are assigned to diamagnetic impurities.

between 6.68 and 7.13 Å for all four pairs (Table S1, Supplementary data).[41a]

In diradical **2**, the structures for the two crystallographically unique molecules show the two nitronyl nitroxide (ONCNO) groups even further apart, with C···C distances of approximately 7.7 Å,[41b] compared to **1** (Table S1, Supplementary data). In each unique molecule, the ONCNO groups are nearly parallel and they form torsional angles of ~30° with the benzene rings within each aryl nitronyl nitroxide moiety.

In both **1** and **2**, the C···C distances of 7–8 Å between the co-facial ONCNO groups are considerably longer than the corresponding N···N distances of 5–6 Å between the co-facial NO groups in the corresponding nitroxide tetraradical and diradical. These increased distances, especially in diradical **2**, are associated with the larger dihedral angles between the co-facial benzene rings that are in the 20–25° range in **1**, in the 36–39° range in **2**, and in the 2.9–14.0° range in the corresponding nitroxide tetraradical and diradical (Table S2, Supplementary data).[41c] This behavior may be caused by the larger steric repulsion of the 4,4,5,5-tetramethylimidazoline-1-oxyl-3-oxide moieties, compared to the *tert*-butylnitroxide moieties at the upper rim of the 1,3-alternate calix[4]arene. Most importantly, the increased radical–radical distances should contribute to the relatively weaker through-space radical–radical interactions in **1** and **2**.

2.3. Structure of 1 and 2 in solution

^{1}H NMR spectra of tetraradical **1** and diradical **2** in chloroform-*d* at room temperature show the expected resonances (Fig. 5, Figs. S4 and S5, Supplementary data). All ^{1}H resonances should be detectable, especially in concentrated solutions, because of the low-to-moderate spin densities at all of the hydrogen atoms in **1** and **2**.[2,42] The reported chemical shifts are not corrected for bulk susceptibility shifts.[43]

Four broad resonances are observed for ~70 mM tetraradical **1** (Fig. 5). The relatively less broadened 12-proton and 24-proton singlets at +5.6 and +4.1 ppm are assigned to the methyl (CH_3) and dimethylene (CH_2CH_2) of the methoxyethyleneoxy ($OCH_2CH_2OCH_3$) groups, respectively; in addition, the +4.1 ppm singlet is assumed to consist of overlapping resonances from the methylene groups of the macrocycle. The two very broad resonances, 8-proton at +22.5 ppm and 48-proton at −13.6 ppm, are assigned to the *ortho*-hydrogens of the benzene rings and the methyl groups of the oxazoline moieties, respectively. Overall, the spectrum provides evidence for a tetraradical with a D_{2d} point group on the NMR time scale.

Five broad resonances, with similar chemical shifts to those in **1**, may be identified for diradical **2**. These resonances may be assigned to the aryl nitronyl nitroxide moieties, as well as to four methylene groups of the macrocycle.[44] In addition, relatively narrow singlets at 7.28, 3.41, and 3.21 ppm are assigned to the aromatic, OCH_3, and OCH_2CH_2O protons of the diamagnetic bromophenyl moieties of **2**, respectively.

The ^{1}H NMR spectral assignments for aryl nitronyl nitroxide moieties in **1** and **2** are similar to those for the corresponding nitronyl nitroxide monoradicals, e.g., 2-phenyl-4,4,5,5-tetramethylimidazoline-1-oxyl-3-oxide, thus confirming the structure of the tetraradical and diradical in solution (Figs. S17 and S18, Supplementary data).[33a] However, the chemical shifts for **1** and **2** are significantly different when compared to the corresponding calix[4]arene nitroxide tetraradical and diradical.[24] Notably, the chemical shifts for the methylene groups of the macrocycle, are about +4 ppm in **1**, compared to −1 ppm in the corresponding nitroxide

tetraradical.[24] This small paramagnetic shift in **1** indicates that the spin density at the hydrogens of the methylene groups in **1** is very small; in the corresponding nitroxide tetraradical the spin density was relatively large and negative, based upon a large upfield paramagnetic shift.

EPR spectra of tetraradical **1** and diradical **2** in toluene/chloroform (4:1) at 296 K show resolved multiplets corresponding to ^{14}N-hyperfine splitting from eight and four nitrogens, respectively (Fig. 6). Adequate simulations of the spectra using a single component, e.g., nitronyl nitroxide tetraradical for **1**, are obtained, confirming high degree of radical purity (99% or higher) of **1** and **2**.[45] The simulation for the diradical is of somewhat lower quality, presumably due to incomplete motional averaging of dipolar couplings. This is consistent with the significantly greater linewidth in the spectra of **2** in solution and greater spectral width for diradical **2** in a rigid matrix, compared to those for tetraradical **1** (Figs. 6 and 7). The ^{14}N-hyperfine couplings lead to peak-to-peak splitting $\Delta H_{pp} \approx 0.188$ mT$=a_N/4$ and $\Delta H_{pp} \approx 0.376$ mT$=a_N/2$ for **1** and **2**, respectively; this corresponds to an identical value of $|a_N|=0.752$ mT for **1** and **2**, which is similar to the value of $|a_N|=0.753$ mT reported for the 4-hydroxyphenyl-substituted nitronyl nitroxide monoradical.[46] These results indicate that nitronyl nitroxides are exchange-coupled with a coupling constant significantly greater than the ^{14}N-hyperfine coupling, $|J/g\mu_B| \gg |a_N|$, i.e., $|J/k| \gg 2$ mK.

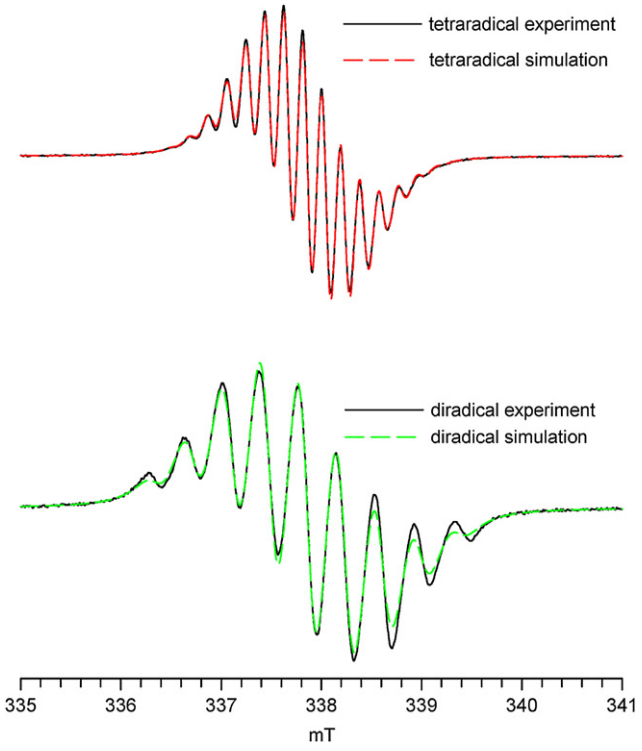

Figure 6. EPR (X-Band) spectra of 0.55 mM tetraradical **1** (top plot) and 0.65 mM diradical **2** (bottom plot) in toluene/chloroform (4:1) at 296 K. Numerical fits (red dashed line) to the experimental spectra correspond to single tetraradical (top plot) and diradical (bottom plot) species; correlation coefficients are 0.999 and 0.995, respectively. The values for the variable parameters for tetraradical are: Lorentzian linewidth of 0.117 mT, g-shift of −0.145 mT (g-value=2.0068), ^{14}N-splitting of 0.188 mT for eight nuclei. The values for the variable parameters for diradical are: Lorentzian linewidth of 0.216 mT, g-shift of −0.147 mT (g-value=2.0065), ^{14}N-splitting of 0.376 mT for four nuclei.

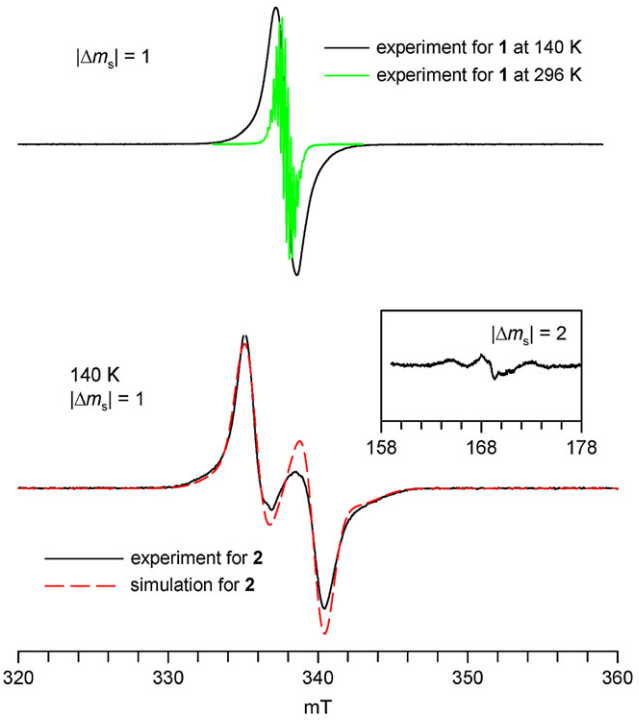

Figure 7. EPR (X-Band) spectra of nitronyl nitroxide tetraradical **1** (0.55 mM, 9.4893 GHz, top plot) and diradical **2** (0.65 mM, 9.4898 GHz, bottom plot) in toluene/chloroform (4:1) at 140 K. For **2**, the spectral simulation of the $|\Delta m_s|=1$ region is shown as red trace. The fitting parameters for the spectral simulation to the $S=1$ state are: $|D/hc|=4.1\times10^{-3}$ cm^{-1}, $|E/hc|=0$ cm^{-1}, $g_x=2.0073$, $g_y=2.0073$, $g_z=2.0035$, Gaussian line ($L_X=1.3$ mT, $L_y=1.7$ mT, $L_z=3.0$ mT).

At 140 K, the EPR spectrum of **1** in toluene/chloroform glass shows a single peak in the $|\Delta m_s|=1$ region, with a peak-to-peak linewidth of about 0.14 mT; the spectral envelope of the $|\Delta m_s|=1$ region is only about doubled in size, compared to the solution phase spectrum for the same sample (Fig. 7). Furthermore, the $|\Delta m_s|=2$ transition could not be detected. These results suggest that tetraradical **1** possesses a rather small zero-field splitting ($|D/hc|$) that is compatible with a relatively high average symmetry for the disposition of nitronyl nitroxide radicals. Similar EPR spectra, consisting of a single peak in the $|\Delta m_s|=1$ region with a peak-to-peak linewidth of about 0.20 mT, were reported for the corresponding nitroxide tetraradical.[24,25]

The EPR spectrum of **2** in toluene/chloroform glass at 140 K possesses four symmetrically disposed broad peaks in the $|\Delta m_s|=1$ region and a barely detectable $|\Delta m_s|=2$ transition. The spectral simulation of the $|\Delta m_s|=1$ region gives $|D/hc|=4.1\times10^{-3}$ cm^{-1} and $|E/hc|=0$ cm^{-1} as zero-field splitting parameters (Fig. 7). The value of $|D/hc|=4.1\times10^{-3}$ cm^{-1} is about three times smaller than $|D/hc|=1.39\times10^{-2}$ cm^{-1} in the corresponding nitroxide diradical.[24] The decrease of $|D/hc|$ may be ascribed to the increased radical–radical distance and greater delocalization of spin density over the ONCNO moiety in **2**. Based upon the point-dipole approximation,[47] the increase of radical–radical distance from 5.5 to 7.5 Å, as estimated by X-ray crystallography, should contribute to the decrease of $|D/hc|$ by a factor of 2.5.

The two outermost peaks are especially broad in **2**, as estimated by the Gaussian linewidth of 0.30 mT in the spectral

simulation (Fig. 7). Analogously to the corresponding nitroxide diradical, this broadness may be associated with the unresolved ^{14}N-hyperfine coupling, suggesting that the nitronyl nitroxide moieties in **2** may be adopting approximately cofacial conformation in toluene/chloroform glass.[24]

The EPR spectra support structural assignments for **1** and **2**, and provide the lower bound estimate for $|J/k| \gg 2$ mK, similar to that in the corresponding nitroxide tetraradical and diradical. An approximate upper bound for $|J|$ may be determined by magnetic studies of **1** and **2**.

2.4. Magnetic studies of 1 and 2 in solution and in the solid state

Magnetization (M) is measured as a function of magnetic field (H=0–5×10^4 Oe and T=1.8, 3, and 5 K) and temperature (T=1.8–300 K at H=30,000, 5000, or 500 Oe). The M versus H and M versus T data are plotted as the M/M_{sat} versus H/T and the χT versus T, respectively, where M_{sat} is the magnetization at saturation and χ is the paramagnetic susceptibility.

For tetraradical **1** and diradical **2** in chloroform, the value of χT is constant in the 30–150 K range, with values of χT=1.49 and 0.72–0.73 emu K mol^{-1} for **1** and **2**, respectively (Fig. 8 and Fig. S6, Supplementary data). Similarly, the ^{1}H NMR-based Evans method gives quantitative values of $\chi T \approx 1.3$–1.5 and 0.8 emu K mol^{-1} for **1** and **2** in chloroform at room temperature (295–300 K), respectively. Within accuracy of the Evans method,[43] these values are in good agreement with the values of χT at T>30 K for solids **1** and **2** (Figs. 9 and 10). These values of χT at high temperatures, T>30 K, are in excellent agreement with the theoretical, spin-only χT=1.50 and 0.75 emu K mol^{-1} for tetraradicals and diradicals, with independent S=1/2 radicals.

At low temperatures, the χT versus T plots for **1** and **2** in the solid state show downward turns, consistent with antiferromagnetic exchange coupling, corresponding to a mean-field parameters, $\theta \approx -0.5$ and -0.3 K, respectively. In order to distinguish whether these exchange couplings are intramolecular or intermolecular, magnetic data in the solid state and in dilute solutions at low temperature ranges should be compared.[24] However, the studies of **1** and **2** in solution are constrained by their low solubility in common organic solvents and magnetic data in solution could only be obtained in chloroform. The χT versus T plots for T<30 K could not be obtained because of the apparent time-dependent magnetic behavior of the radicals in a chloroform matrix. Therefore, low temperature magnetic data can only be obtained at constant temperature, after long annealing of the matrix at each temperature. In this way, the M/M_{sat} versus $H/(T-\theta)$ plots at T=1.8, 3, and 5 K were obtained

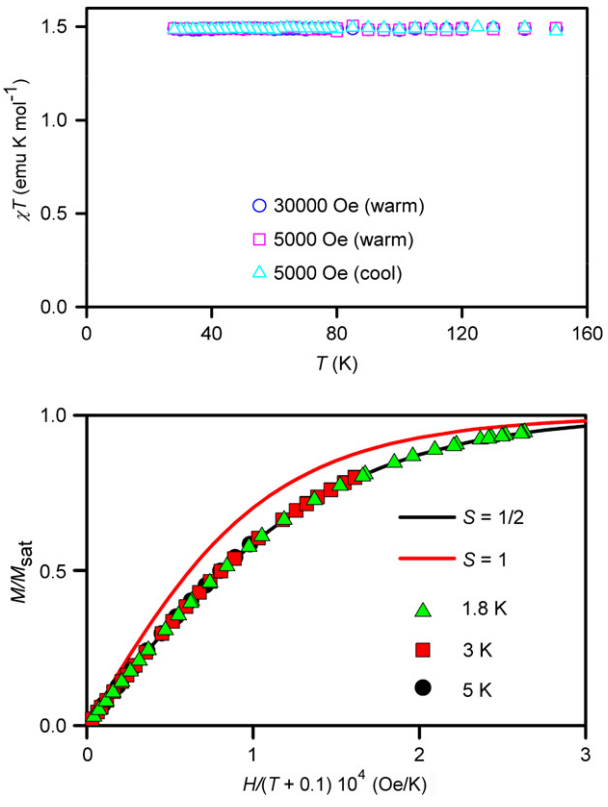

Figure 8. SQUID magnetometry for 5 mM tetraradical **1** in $CHCl_3$. Top plot corresponds to χT versus T in both cooling and warming modes, with χT=1.49 emu K mol^{-1} in the high temperature range. Bottom plot corresponds to M/M_{sat} versus $H/(T-\theta)$, with solid lines showing plots of Brillouin functions with S=1/2 and S=1; numerical fits to the Brillouin functions with θ=−0.1 K give S=0.50 and M_{sat}=0.98 μ_B at 1.8, 3, and 5 K.

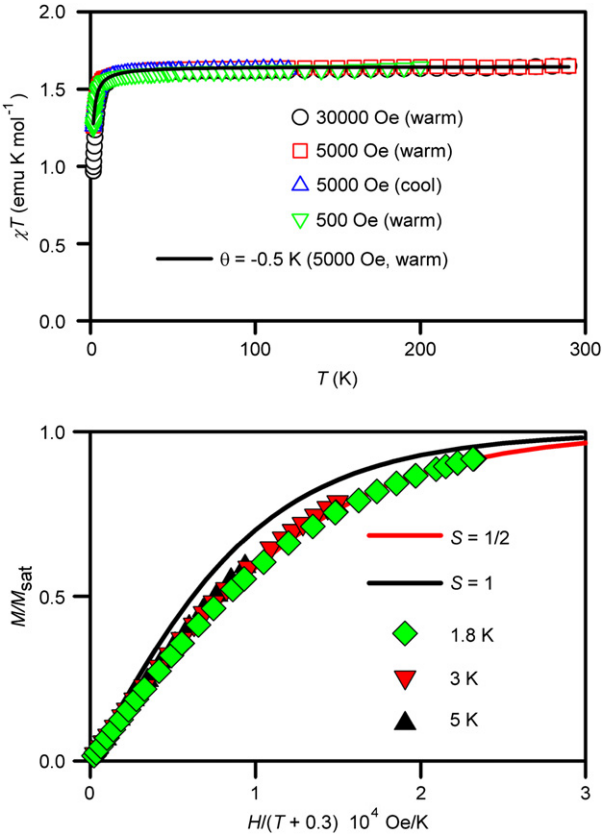

Figure 9. SQUID magnetometry for polycrystalline tetraradical **1**. Top plot corresponds to χT versus T in both cooling and warming modes; the solid line shows a numerical fit to the S=1/2 Brillouin function with θ=−0.5 K. Bottom plot corresponds to M/M_{sat} versus $H/(T-\theta)$, with solid lines showing plots of Brillouin functions with S=1/2 and S=1; numerical fits to the Brillouin functions with θ=−0.3 K give $S \approx 0.5$ and $M_{sat} \approx 1.0$ μ_B at 1.8 and 3 K.

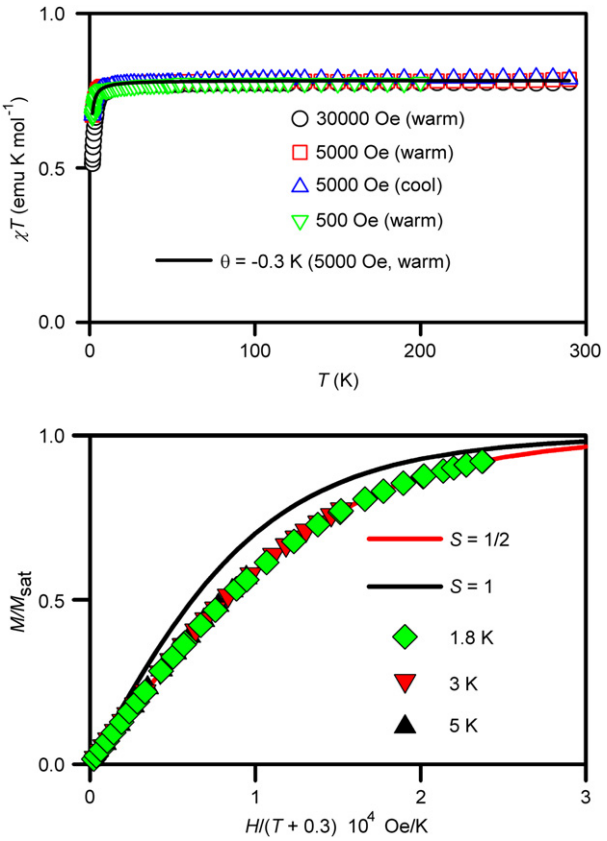

Figure 10. SQUID magnetometry for polycrystalline diradical **2**. Top plot corresponds to χT versus T in both cooling and warming modes; the solid line shows a numerical fit to the $S=1/2$ Brillouin function with $\theta=-0.3$ K. Bottom plot corresponds to M/M_{sat} versus $H/(T-\theta)$, with solid lines showing plots of Brillouin functions with $S=1/2$ and $S=1$; numerical fits to the Brillouin functions with $\theta=-0.3$ K give $S\approx0.50$ and $M_{sat}\approx1.0$ μ_B at 1.8 and 3 K.

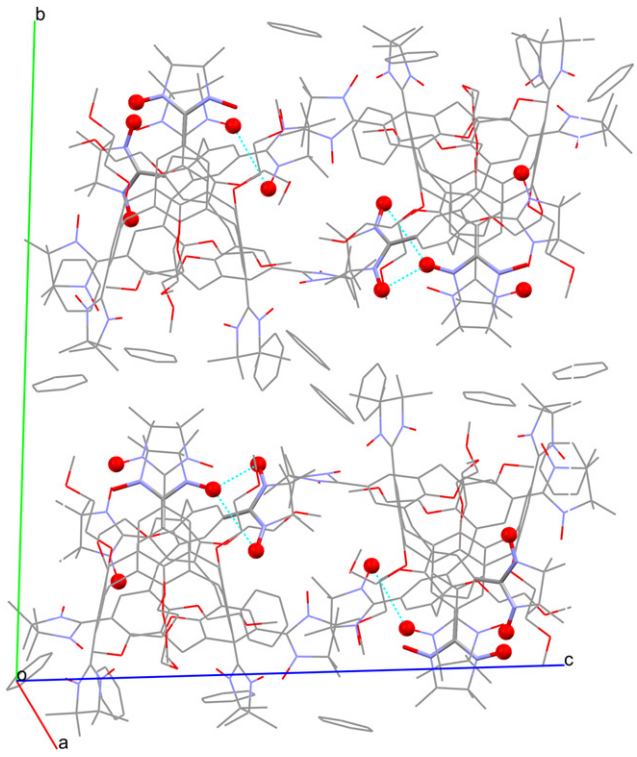

Figure 11. Crystal packing of nitroxide tetraradical **1**. Disorder and hydrogen atoms are omitted for clarity. Oxygen atoms with short radical–radical O···O distances, 3.607–4.088 Å, are depicted as ball-and-stick model. Pairs of the ONCNO moieties connected with two short O···O distances are depicted as stick model.

for 5 mM **1** in chloroform and 20 mM **2** in chloroform (Fig. 8 and Fig. S6); for both **1** and **2**, $\theta\approx-0.1$ K, with $S\approx0.5$ and M_{sat}=0.9–1.0 μ_B, is obtained.[48] These values of θ may be compared to $\theta\approx-0.3$ K, as well as $S\approx0.5$ and $M_{sat}\approx1.0$ μ_B, obtained from analogous plots for **1** and **2** in the solid state (Figs. 9 and 10).

These results indicate that antiferromagnetic exchange coupling between the radicals in **1** and **2** is very small and most likely intermolecular. In chloroform solution, the magnetic data for both **1** and **2** resemble paramagnetic behavior of four and two independent spins $S=1/2$, respectively, even at the lowest measurement temperature of 1.8 K. This provides the upper limit of $|J/k|\ll0.5$ K, most likely $|J/k|<0.2$ K, for the strength of intramolecular exchange coupling between the radicals.

2.5. Crystal packing of 1

The crystal packing of tetraradical **1** may be described in terms of alternating layers of calix[4]arene macrocycles and benzene molecules in the approximate *ac*- or (010)-planes (Fig. 11, Figs. S1–S3, Supplementary data).

For **1**, multiple intermolecular radical–radical O···O distances in the 3.6–4.1 Å range may be identified within each layer of macrocycles. One pair of nitronyl nitroxides has relatively short radical–radical O···O distance, O2A–O6B=3.607 Å. Another pair of nitronyl nitroxides possesses radical–radical O···O distances of O10A–O1B=3.636 Å and O10A–O2B=4.088 Å. For both pairs, significant antiferromagnetic exchange coupling is expected, and in the second pair, exchange coupling may be amplified by the presence of two parallel exchange coupling pathways.[49] Intermolecular antiferromagnetic exchange coupling may contribute to the more negative values of the mean-field parameter θ for the magnetic data of **1** in the solid state.

3. Radical–*m*-phenylene–C(sp^3)–*m*-phenylene–radical exchange coupling pathway

In 2000, Frank and co-workers reported the synthesis and characterization of a nitronyl nitroxide-based spiroconjugated diradical, shown in Figure 12.[50] The magnetic studies of the diradical in the solid state indicated a relatively large antiferromagnetic exchange coupling, which was assigned to the through-bond exchange coupling with the coupling constant $J/k=-3$ K (singlet–triplet gap, $2|J/k|=6$ K).[50] In addition, plots of the EPR signal intensity versus $1/T$ for the diradical in dilute organic matrices showed curvatures at low temperatures that were consistent with $J/k\approx-3$ K.[50] These values of $|J/k|$ are larger by at least one order of magnitude than $|J/k|\ll0.5$ K, determined for nitronyl nitroxide tetraradical **1**. It should be noted that the through-bond exchange coupling pathway, radical–*m*-phenylene–C(sp^3)–*m*-phenylene–radical, in the spiroconjugated

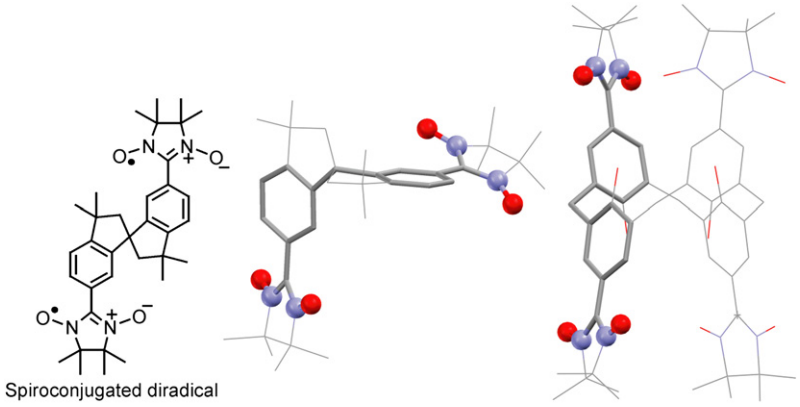

Figure 12. The nitronyl nitroxide–*m*-phenylene–C(sp^3)–*m*-phenylene–nitronyl nitroxide exchange coupling pathways (displayed as stick model) in spiroconjugated diradical and in 1,3-alternate calix[4]arene tetraradical **1**. The NO moieties are shown as stick-and-ball model. Hydrogen atoms and methoxyethylene chains in tetraradical **1** are omitted for clarity.

diradical and tetraradical **1** is identical but the conformations of the exchange coupling pathways are significantly different (Fig. 12).[24] However, it might be possible that the intermolecular exchange coupling in the solid state (in the magnetic studies) and the microwave saturation at low temperatures in the EPR studies significantly affected the reported $J/k \approx -3$ K.[51–53]

4. Conclusion

Exchange coupling in 1,3-alternate calix[4]arene nitronyl nitroxide tetraradical and diradical was studied. In the solid state, weak antiferromagnetic coupling, that is stronger than the one in solution, is found between neighboring molecules. In solution, the exchange coupling constants ($|J/k|$) are much larger than ^{14}N-hyperfine splitting for nitronyl nitroxides but they are much smaller than those determined for the corresponding nitroxide radicals, i.e., $0.5\ \text{K} \gg |J/k| \gg 2$ mK. Much weaker intramolecular exchange coupling in the nitronyl nitroxide tetraradical and diradical, compared to that in the corresponding nitroxide tetraradical and diradical, correlates to their distinct structures and spin density distributions. 1,3-Alternate calix[4]arene nitronyl nitroxide tetraradical and diradical provide a model system for the study of electron spin relaxation in the presence of weak radical–radical interactions.

5. Experimental section

5.1. Materials and special procedures

Ether, tetrahydrofuran (THF), and 2-methyltetrahydrofuran (2-MeTHF) were freshly distilled from sodium/benzophenone prior to use. *n*-BuLi in hexane and *t*-BuLi in pentane were obtained from either Aldrich or Acros; concentration of the organolithiums was determined by titration with *N*-pivaloyl-*o*-toluidine.[54] Perdeuterated solvents for NMR spectroscopy were obtained from Cambridge Isotope Laboratories. All other commercially available chemicals were obtained from Aldrich or Acros. Prior to use, benzaldehyde and *p*-anisaldehyde were subjected to the general method for purification of aldehydes.[55] 5,11,17,23-Tetrabromo-25,26,27,28-tetrakis(methoxyethoxy)calix[4]arene (**3**) in the locked 1,3-alternate conformation[37] was prepared using previously reported procedures.[24] 2,3-Bis(hydroxyamino)-2,3-dimethylbutane was obtained by reduction of the corresponding dinitro compound using Al/Hg.[39] Column chromatography was carried out with flash silica gel, particle size 40–63 μm, obtained from EMD chemicals or with TLC grade silica gel (Aldrich) using 0–20 psig pressure. Preparative TLC (PTLC) was carried out using Analtech silica plates (tapered with a preadsorbent zone). Standard Schlenk techniques for synthesis under inert atmosphere were employed.

5.2. NMR spectroscopy and other analyses

NMR spectra were obtained in $CDCl_3$ or DMSO-d_6 using Bruker spectrometers (^{1}H, 400 and 600 MHz). The chemical shift references were as follows: (^{1}H) $CHCl_3$, 7.26 ppm; (^{13}C) $CDCl_3$, 77.0 ppm ($CDCl_3$); (^{1}H) DMSO-d_5, 2.50 ppm; (^{13}C) DMSO-d_5, 38.50 ppm (DMSO-d_6). Typical 1D FID was subjected to exponential multiplication with an exponent of 0.1 Hz (for ^{1}H) and 1.0–2.0 Hz (for ^{13}C). Values of the magnetic moment and χT were obtained in chloroform using the ^{1}H NMR-based Evans method.[43] Concentric NMR tubes were used (Wilmad, cat. No. WGS-5BL). The outer NMR tube contained a solution of the paramagnetic sample in an approximately 1:1 (v/v) mixture of $CDCl_3$ and $CHCl_3$ with accurately determined concentration and the inner concentric tube contained pure $CHCl_3$. Diamagnetic susceptibility of $CHCl_3$ ($\chi_{dia} = -0.497 \times 10^{-6}$ emu g^{-1}) was used. IR spectra were obtained using a Nicolet Avatar 360 FTIR instrument, equipped with an ATR sampling accessory (Spectra Tech, Inc.). A few drops of the compound in CH_2Cl_2 were applied to the surface of a ZnSe ATR plate horizontal parallelogram (45°, Wilmad). After the solvent evaporated, the spectrum was acquired (128 scans, 4 cm^{-1} resolution). FABMS analyses were carried out at the Nebraska Center for Mass Spectrometry, using 3-nitrobenzyl alcohol (3-NBA) as a matrix.

5.3. X-ray crystallography

Crystals of **1** and **2** were obtained by slow evaporation of benzene/heptane.

The data were collected on a Bruker SMART6000 system at the Indiana University and at beamline 15ID,

ChemMatCARS, at the Advanced Photon Source, Argonne National Laboratory in Chicago. For the data collection, single crystals were placed onto the tip of a 0.1 mm diameter glass capillary.

Additional description of the X-ray crystallographic data may be found in Refs. 40 and 41, as well as in the Supplementary data.

5.4. EPR spectroscopy

CW X-band EPR spectra for **1** and **2** in solution were acquired on Bruker EMX instrument, equipped with a frequency counter and nitrogen flow temperature control (130–300 K). The samples were contained in 4-mm O.D. EPR quartz tubes, equipped with high-vacuum PTFE stopcocks. Solvent was vacuum transferred into the tube, to form a homogeneous solution after attaining ambient temperature. Spectra were obtained using dual mode cavity, with the oscillating magnetic field perpendicular (TE_{102}) to the swept magnetic field. The *g*-values were referenced using DPPH (g=2.0037, powder, Aldrich).

5.5. SQUID magnetometry

Quantum Design (San Diego, CA) MPMS5S (with continuous temperature control) was used.

For solution samples, tetraradical **1** or diradical **2** was loaded into homemade 5-mm O.D. EPR quality quartz tubes, equipped with high-vacuum PTFE stopcocks. The tubes were modified to possess a thin bottom, which is 6 cm from the end of the tube.[18,24] The tube was placed under vacuum, and then solvent was vacuum transferred. After the tube was flame sealed under vacuum, the frozen samples were rapidly inserted from liquid nitrogen to the magnetometer, with the sample chamber at 10 K, using the well-established procedure for polyarylmethyl polyradicals.[18] Subsequently, a sequence of measurements below the softening point of the matrix (1.8–150 K) were carried out. Correction for diamagnetism was implemented by extrapolation of the χ versus $1/T$ plots, typically, from the 70–140 K temperature range (R^2= 0.9999). In most cases, the warming mode data, with 60-s delays, after a 'stable temperature' was indicated by the MPMS at each temperature, were used for such extrapolations.

For solid state samples, polycrystalline tetraradical **1** or diradical **2** (18–21 mg) was loaded to the 3-piece gelatin capsule. Following the measurements, the capsule was partially emptied (7–8 mg of radical left), and then identical sequences of measurements were carried out for the point-by-point correction for diamagnetism. Additional correction was based upon Pascal constants: $\chi_{dia}=7.84\times 10^{-4}$ emu mol^{-1} (for **1**) and $\chi_{dia}=6.59\times 10^{-4}$ emu mol^{-1} (for **2**).[56]

5.6. EPR spectral simulations and numerical curve fitting for SQUID magnetic data

The WINEPR SimFonia program (Version 1.25, Bruker) was used for spectral simulations of nitronyl nitroxide diradical **2** in rigid matrices. WinSIM program (Public EPR Software Tools, D. A. O'Brien, D. R. Duling, Y. C. Fann) was used for numerical fitting of solution phase EPR spectra. The SigmaPlot for Windows software package was used for numerical curve fitting of the magnetic data. The reliability of a fit is measured by the parameter dependence, which is defined as follows: *dependence=1−((variance of the parameter, other parameters constant)/(variance of the parameter, other parameters changing))*. Values close to 1 indicate an overparametrized fit.

5.7. Tetraaldehyde 4: 5,11,17,23-tetraformyl-25,26,27,28-tetrakis(methoxyethoxy)calix[4]arene[38]

t-BuLi in pentane (titrated, 1.58 M, 1.57 mL, 2.5 mmol) was added to a solution of tetrabromocalix[4]arene **3** (0.301 g, 0.310 mmol) in THF (20 mL) at −78 °C. The resultant bright orange solution was stirred at −78 °C for 2 h, and then warmed up to −20 °C for 15 min. The reaction was re-cooled to −78 °C, and neat *N*-methylformanilide (0.168 g, 1.24 mmol) was added. The reaction mixture was left to warm up to room temperature overnight. It was then taken up in excess chloroform (~100 mL), and the organic layer was washed with water (3×50 mL) and dried with $MgSO_4$. Evaporation of the solvent and flash chromatography (silica, 20–25% ethyl acetate in benzene) gave tetraaldehyde **4** (189.5 mg, 79%). From two other reactions carried out using 100.0 and 401.7 mg of the tetrabromocalix[4]arene **3**, tetraaldehyde **4** was obtained in 51% (40.3 mg) and 70% (0.222 g) yields, respectively; for these two reactions, purification was based upon triturating the crude with ether. Mp 172–174 °C (under N_2). ^{1}H NMR (400 MHz, $CDCl_3$): δ 9.673 (s, 4H, C*H*O), 7.657 (s, 8H, Ar*H*), 3.997 (m, 8H, OCH_2), 3.871 (m, 8H, OCH_2), 3.633 (s, 8H, ArCH_2), 3.621 (s, 12H, OCH_3). ^{13}C NMR (100 MHz, $CDCl_3$): δ 191.8, 160.7, 133.9, 132.0, 131.0, 72.7, 71.9, 59.0, 33.3. IR (ZnSe, cm^{-1}): 2980, 2933, 2878, 1684, 1587, 1452, 1432, 1308, 1274, 1222, 1120, 1052, 1027. The ^{1}H and ^{13}C NMR spectra were coinciding with those previously reported for tetraaldehyde **4**.[38]

5.8. Dialdehyde 5: 5,17-diformyl-11,23-dibromo-25,26,27,28-tetrakis(methoxyethoxy)calix[4]arene

n-BuLi in hexane (titrated, 2.45 M, 0.52 mL, 1.30 mmol) was added to a solution of tetrabromocalix[4]arene **3** (0.614 g, 0.630 mmol) in THF (37 mL) at −78 °C. The resultant orange solution was stirred at −78 °C for 2 h, and then warmed to −20 °C for 15 min. The color of the solution changed to a dark red. The reaction mixture was then cooled to −78 °C, and then neat *N*-methylformanilide (0.204 g, 1.51 mmol) was added, to give a colorless solution. The reaction mixture was left to warm up to room temperature overnight. After removal of solvents under reduced pressure, a yellow residue was obtained, and then dissolved in dichloromethane; the organic layer was then washed with distilled water three times. The organic layer was dried over $MgSO_4$ and concentrated in vacuo to give yellowish-white crude (0.795 g). This crude was combined with the crude (1.108 g) from another reaction carried out on 1.0 g of the tetrabromocalix[4]arene **3**, and then purified by flash chromatography (silica, 5–10% ether in chloroform) to yield dialdehyde **5** (0.699 g, 48%). Column chromatography of the combined crudes from two other reactions, done on 50.0 and 0.500 g of the tetrabromocalix[4]arene **3**, followed by

treatment with ether, gave dialdehyde **5** (0.181 g, 37%). Mp 217–220 °C (under N_2). ^{1}H NMR (400 MHz, $CDCl_3$): δ 9.683 (s, 2H, C*H*O), 7.662 (s, 4H, Ar*H*), 7.323 (s, 4H, Ar*H*), 3.927 (m, 8H, OCH_2), 3.83–3.79 (m, 8H, OCH_2), 3.622 (s, 3H, OCH_3), 3.594 (s, 3H, OCH_3), 3.595, 3.502 (AB, J= 13 Hz, 8H, ArCH_2). ^{13}C NMR (100 MHz, $CDCl_3$): δ 191.8, 160.7, 154.4, 134.6, 133.7, 133.0, 132.5, 130.7, 115.2, 72.4, 72.3, 71.9, 71.9, 59.3, 59.0, 33.7. HR-FABMS (3-NBA matrix) *m*/*z* (ion type, % RA for *m*/*z*=868–875, deviation for the formula): 874.1553 ([M+2H+4]$^+$, 22%, 2.4 ppm for $^{12}C_{42}{}^{1}H_{48}{}^{16}O_{10}{}^{81}Br_2$), 874.1553 ([M+H+5]$^+$, 22%, −2.8 ppm for $^{12}C_{41}{}^{13}C_1{}^{1}H_{47}{}^{16}O_{10}{}^{81}Br_2$), 873.1507 ([M+H+4]$^+$, 58%, −1.4 ppm for $^{12}C_{42}{}^{1}H_{47}{}^{16}O_{10}{}^{81}Br_2$), 872.1516 ([M+H+3]$^+$, 57%, 3.7 ppm for $^{12}C_{41}{}^{13}C_1{}^{1}H_{47}{}^{16}O_{10}{}^{79}Br_1{}^{81}Br_1$), 871.1508 ([M+H+2]$^+$, 100%, 0.9 ppm for $^{12}C_{42}{}^{1}H_{47}{}^{16}O_{10}{}^{79}Br_1{}^{81}Br_1$), 871.1508 ([M+3]$^+$, 100%, −4.3 ppm for $^{12}C_{41}{}^{13}C_1{}^{1}H_{46}{}^{16}O_{10}{}^{79}Br_1{}^{81}Br_1$), 870.1483 ([M+2]$^+$, 57%, −5.2 ppm for $^{12}C_{42}{}^{1}H_{46}{}^{16}O_{10}{}^{79}Br_1{}^{81}Br_1$), 869.1514 ([M+H]$^+$, 54%, 2.5 ppm for $^{12}C_{42}{}^{1}H_{47}{}^{16}O_{10}{}^{79}Br_2$), 869.1514 ([M+1]$^+$, 54%, −2.6 ppm for $^{12}C_{41}{}^{13}C_1{}^{1}H_{46}{}^{16}O_{10}{}^{79}Br_2$), 868.1445 ([M]$^+$, 17%, 1.4 ppm for $^{12}C_{42}{}^{1}H_{46}{}^{16}O_{10}{}^{79}Br_2$). IR (ZnSe, cm^{-1}): 2979, 2923, 2886, 1689, 1597, 1588, 1450, 1306, 1200, 1124, 1054, 1029.

5.9. Tetrakis(1,3-dihydroimidazolidine) 6: 5,11,17,23-tetrakis(1,3-dihydroxy-4,4,5,5-tetramethylimidazolin-2-yl)-25,26,27,28-tetrakis(methoxyethoxy)calix[4]arene

A mixture of tetraaldehyde **4** (0.173 g, 0.224 mmol), 2,3-bis(hydroxyamino)-2,3-dimethylbutane (0.327 g, 2.21 mmol), *p*-TsOH·H_2O (8.4 mg, 0.044 mmol) was evacuated in a Schlenk flask for 30 min. Subsequently, methanol (1.0 mL) was added under N_2, and then the Schlenk flask was transferred to an oil bath at 60–65 °C. The progress of the reaction, it took between 2 and 2.5 days to complete, was followed by TLC (silica, ether/hexanes); the tetra-condensation product had $R_f \approx 0$, even in acetone and in acetonitrile. The crude was then washed with water (2×3 mL), ethanol containing a drop of Et_3N (1×2 mL), and ether (3×1 mL) to give tetrakis(1,3-dihydroimidazolidine) **6** as a white solid (0.227 g, 79%). From two other reactions done on 51.0 mg of the tetraaldehyde **4** with methanol (2 mL) and heating at 65–75 °C, and 0.175 g of the tetraaldehyde **4** with methanol (2 mL) and heating at 60–65 °C, **6** was obtained in 91% (0.078 g) and 85% (0.250 g) yields, respectively. Mp ~270 °C (under N_2, dec). ^{1}H NMR (400 MHz, DMSO-d_6): δ 7.605 (s, 8H, O*H*, exch D_2O), 7.196 (s, 8H, Ar*H*), 4.497 (s, 4H, C*H*), 3.847 (s, 8H, ArCH_2), 3.355 (s, 8H, OCH_2, under the H_2O peak from solvent), 3.104 (s, 12H, OCH_3), 2.940 (t, 5.2 Hz, 8H, OCH_2), 1.071 (s, 12H, CH_3), 0.974 (s, 12H, CH_3). ^{13}C NMR (100 MHz, DMSO-d_6): δ 156.3, 135.5, 133.1, 129.0, 90.4, 70.9, 69.4, 66.4, 58.7, 38.4, 25.0, 17.6. LR-FABMS (3-NBA matrix) *m*/*z*: calculated for $C_{68}H_{104}N_8O_{16}$ [M]$^+$ 1289.6; found 1289.6. IR (ZnSe, cm^{-1}): 3269, 2977, 2926, 1453, 1364, 1203, 1118.

5.10. Bis(1,3-dihydroimidazolidine) 7: 5,17-bis(1,3-dihydroxy-4,4,5,5-tetramethylimidazolin-2-yl)-11,23-dibromo-25,26,27,28-tetrakis(methoxyethoxy)calix[4]-arene

A mixture of dialdehyde **5** (0.100 g, 0.115 mmol), 2,3-bis-(hydroxyamino)-2,3-dimethylbutane (85.2 mg, 0.575 mmol), *p*-TsOH·H_2O (8.2 mg, 0.043 mmol) was evacuated in a Schlenk flask for 30 min. Subsequently, methanol (0.5 mL) was added under N_2, and then the Schlenk vessel was transferred to an oil bath at 55–60 °C. The progress of the reaction, for which it took between 2–3 days to complete, was determined by TLC (silica, ether/hexanes); the di-condensation product had $R_f \approx 0$ in acetone and in acetonitrile. The crude was then washed with water (2×2 mL), ethanol containing a drop of Et_3N (1×1 mL), and ether (3×1 mL), to give bis(1,3-dihydroimidazolidine) **7** as a white solid (0.115 g, 88%). From another reaction carried out on 0.153 g of the dialdehyde **5**, bis(1,3-dihydroimidazolidine) **7** (0.165 g, 90%) was obtained. ^{1}H NMR (600 MHz, DMSO-d_6): δ 7.706 (s, 4H, O*H*, exch D_2O), 7.292 (s, 4H, Ar*H*), 7.160 (s, 4H, Ar*H*), 4.444 (s, 4H, C*H*), 3.818, 3.796 (AB, J=16.2 Hz, 8H, ArCH_2), 3.597 (t, J=6.6 Hz, 8H, OCH_2), 3.329 (s, 6H, OCH_3), 3.16–3.14 (br m, 4H, OCH_2), 3.085 (s, 6H, OCH_3), 3.024 (t, J=7.2 Hz, 4H, OCH_2), 1.053 (s, 6H, CH_3), 1.007 (s, 6H, CH_3). ^{13}C NMR (150 MHz, DMSO-d_6): 155.8, 155.0, 136.3, 135.9, 132.7, 131.5, 128.9, 113.7, 89.8, 71.3, 70.6, 69.7, 67.3, 66.0, 58.5, 58.3, 36.6, 24.6, 17.2. LR-FABMS (3-NBA matrix) *m*/*z*: calculated for $C_{54}H_{75}Br_2N_4O_{12}$ [M+H]$^+$ 1132.0; found 1131.5. IR (ZnSe, cm^{-1}): 3433, 3335, 2980, 2924, 1454, 1358, 1207, 1123, 1058, 1028, 845.

5.11. Nitronyl nitroxide tetraradical 1: 5,11,17,23-tetrakis(1-oxyl-3-oxo-4,4,5,5-tetramethylimidazolin-2-yl)-25,26,27,28-tetrakis(methoxyethoxy)calix[4]arene

Tetrakis(1,3-dihydroimidazolidine) **6** (0.225 g, 0.174 mmol) was suspended in CH_2Cl_2 (10 mL), and the suspension was cooled to a temperature between −5 and 0 °C. Subsequently, a solution of $NaIO_4$ (0.150 g, 0.696 mmol) in distilled water (15 mL) was added. The very light blue reaction mixture was stirred at −5 to 0 °C for 35 min, and then at room temperature for an additional 30 min, resulting in a dark blue reaction mixture. The completion of reaction was determined by TLC (silica, ethyl acetate/acetone), as indicated by the disappearance of starting material and the appearance of a blue spot for tetraradical **1**. The work up was carried out by the addition of CH_2Cl_2 (40 mL) and then washing of the organic layer with water (3×30 mL). The organic layer was then dried over $MgSO_4$, filtered, evaporated, and then flash chromatographed (silica, 10–20% acetone in ethyl acetate) to give **1** (80.1 mg). Further purification by crystallization from benzene/heptane gave 63.3 mg (28% from two crops) of **1**. Another reaction, which was carried out at room temperature using 65.4 mg of **6**, gave tetraradical **1** (15.0 mg, 23%), after two successive recrystallizations. Mp ~200 °C (under N_2, dec). ^{1}H NMR (600 MHz, $CDCl_3$, 68 mM): δ 22.5 (v. br s, 8H, Ar*H*), 5.63 (br s, 12H), 4.09 (br s, 24H), −13.6 (v. br s, 48H, C(CH_3)$_2$). LR-FABMS (3-NBA matrix) cluster: *m*/*z* (% RA for *m*/*z*=500–2000) at (M)$^+$ 1277.6 (13), 1278.6 (15), 1279.6 (17), 1280.6 (15), 1281.6 (8), at (M−O)$^+$ 1261.5 (25), 1262.5 (36), 1263.5 (31), 1264.5 (22), 1265.5 (13), at (M−2O)$^+$ 1245.6 (25), 1246.5 (68), 1247.5 (65), 1248.5 (42), 1249.5 (26), at (M−3O)$^+$ 1230.5 (88), 1231.5 (100), 1232.5 (70), 1233.5 (38), at (M−4O)$^+$ 1212.5 (14), 1213.5 (27), 1214.5 (68), 1215.5 (85), 1216.5 (72), 1217.5 (41), 1218.5 (17), at (M−5O)$^+$ 1197.5 (12), 1198.5 (22), 1199.5 (28), 1200.5 (26), 1201.5 (17). HR-FABMS (3-NBA matrix): *m*/*z* (ion

type, % RA in the *m*/*z* 1270–2100, deviation for the formula) at 1282.7082 ([M+6]$^+$, 11.6, 1.4 ppm for $^{12}C_{68}{}^{1}H_{98}{}^{14}N_8{}^{16}O_{16}$), 1281.7126 ([M+5]$^+$, 23.2, 8.1 ppm for $^{12}C_{67}{}^{13}C^{1}H_{97}{}^{14}N_8{}^{16}O_{16}$), 1280.7063 ([M+4]$^+$, 42.8, 9.3 ppm for $^{12}C_{68}{}^{1}H_{97}{}^{14}N_8{}^{16}O_{16}$), 1279.6958 ([M+3]$^+$, 45.9, 7.2 ppm for $^{12}C_{68}{}^{1}H_{95}{}^{14}N_8{}^{16}O_{16}$), 1278.6907 ([M+2]$^+$, 45.3, 9.3 ppm for $^{12}C_{68}{}^{1}H_{94}{}^{14}N_8{}^{16}O_{16}$), 1277.6826 ([M+1]$^+$, 41.4, 9.1 ppm for $^{12}C_{68}{}^{1}H_{93}{}^{14}N_8{}^{16}O_{16}$), 1276.6679 ([M]$^+$, 16.6, 3.8 ppm for $^{12}C_{68}{}^{1}H_{92}{}^{14}N_8{}^{16}O_{16}$). IR (ZnSe, cm^{-1}): 2981, 2925, 1452, 1386, 1356, 1218, 1125. Evans method (two measurements, $CDCl_3/CHCl_3$, 295 or 296 K), χT= 1.3–1.5 emu K mol^{-1} (3.5, 4.1 unpaired electrons).

5.12. Nitronyl nitroxide diradical 2: 5,17-bis(1-oxyl-3-oxo-4,4,5,5-tetramethylimidazolin-2-yl)-11,23-dibromo-25,26,27,28-tetrakis(methoxyethoxy)calix[4]arene

Bis(1,3-dihydroimidazolidine) **7** (0.160 g, 0.141 mmol) was suspended in CH_2Cl_2 (15 mL), and then the suspension was cooled to a temperature between −5 and 0 °C. Subsequently, a solution of $NaIO_4$ (61.7 mg, 0.288 mmol) in distilled water (8 mL) was added. The very light blue reaction mixture was stirred at −5 to 0 °C for 35 min. After the reaction mixture was warmed to 0 °C and stirred for 15 min at 0 °C, the color changed to dark blue. The completion of reaction was determined by TLC (silica, ethyl acetate/ether), as indicated by the disappearance of starting material and appearance of a blue spot for the product **2**. For the work up, the reaction mixture was diluted with additional CH_2Cl_2 (40 mL) and then the organic layer was washed with water (3×30 mL). After drying over $MgSO_4$, filtration, and concentration under vacuo, the crude was purified by flash chromatography (silica, 50% ethyl acetate in ether), to give diradical **2** (89.2 mg). The subsequent recrystallization from ethyl acetate/CH_2Cl_2 provided the final diradical product **2** (66.6 mg, 42% from two crops). From other reactions carried out on 44.8 and 31.2 mg of **7**, 21.8 mg (49% from three crops after recrystallization) and 19.4 mg (63% from two crops after recrystallization) of **2** were obtained, respectively. Mp ~200 °C (under N_2, dec). ^{1}H NMR (400/600 MHz, $CDCl_3$): δ 19.5 (br s, 4H, Ar*H*), 7.280 (s, 4H, Ar*H*), 6.32, 4.874, 4.18 (br s, s, br s, 22H), 3.412 (s, 8H), 3.207 (s, 6H), −14.3 (br s, 24H, $C(CH_3)_2$). LR-FABMS (3-NBA matrix) cluster: *m*/*z* (% RA for *m*/*z*=1000–2000) at (M)$^+$ 1123.2 (34), 1124.2 (45), 1125.2 (65), 1126.2 (54), 1127.2 (49), 1128.2 (36), at (M−O)$^+$ 1107.2 (34), 1108.2 (45), 1109.2 (64), 1110.2 (73), 1111.2 (54), 1112.2 (42), and at (M−2O)$^+$ 1092.1 (51), 1093.1 (67), 1094.1 (100), 1095.1 (93), 1096.1 (73), 1096.1 (49). HR-FABMS (3-NBA matrix): *m*/*z* (ion type, % RA in the *m*/*z* 1120–2000, deviation for the formula) at 1128.3372 ([M+6]$^+$, 29.3, 5.0 ppm for $^{12}C_{54}{}^{1}H_{70}{}^{14}N_4{}^{16}O_{12}{}^{81}Br_2$), 1127.3312 ([M+5]$^+$, 49.0, 5.1 ppm for $^{12}C_{53}{}^{13}C^{1}H_{70}{}^{14}N_4{}^{16}O_{12}{}^{79}Br^{81}Br$), 1126.3340 ([M+4]$^+$, 61.1, 0.3 ppm for $^{12}C_{54}{}^{1}H_{70}{}^{14}N_4{}^{16}O_{12}{}^{79}Br^{81}Br$), 1125.3293 ([M+3]$^+$, 70.2, 3.1 ppm for $^{12}C_{54}{}^{1}H_{69}{}^{14}N_4{}^{16}O_{12}{}^{81}Br^{79}Br$), 1124.3314 ([M+2]$^+$, 39.1, 0.2 ppm for $^{12}C_{53}{}^{13}C^{1}H_{69}{}^{14}N_4{}^{16}O_{12}{}^{79}Br_2$), 1123.3290 ([M+1]$^+$, 32.6, 1.0 ppm for $^{12}C_{54}{}^{1}H_{69}{}^{14}N_4{}^{16}O_{12}{}^{79}Br_2$), 1122.3238 ([M]$^+$, 9.9, 3.4 ppm for $^{12}C_{54}{}^{1}H_{68}{}^{14}N_4{}^{16}O_{12}{}^{79}Br_2$). IR (ZnSe, cm^{-1}): 2983, 2922, 2875, 1452, 1387, 1357, 1127. Evans method (one measurement, $CDCl_3$/$CHCl_3$, 296 K), χT=0.79 emu K mol^{-1} (2.1 unpaired electrons).

Acknowledgements

This research was supported by the National Science Foundation (CHE-0414936), including the purchase of the Electron Paramagnetic Resonance (EPR) spectrometer (DMR-0216788). Part of this research was performed in facilities renovated with support from NIH (RR16544-01). ChemMatCARS Sector 15 is principally supported by the National Science Foundation/Department of Energy under grant number CHE-0087817. The Advanced Photon Source is supported by the U.S. Department of Energy, Basic Energy Sciences, Office of Science, under Contract No. W-31-109-Eng-38. We thank Dr. Kouichi Shiraishi for help with the EPR spectroscopy and preparation of samples for SQUID magnetometry.

Supplementary data

General procedures and materials, additional crystallographic data for **1** and **2**, SQUID magnetometry data for diradical **2** in chloroform, preparation of 2,3-bis(hydroxyamino)-2,3-dimethylbutane and nitronyl nitroxide monoradicals, IR, ^{1}H NMR and ^{13}C NMR spectra for selected compounds **1**–**7**. The supplementary data associated with this article can be found in the online version, at doi:10.1016/j.tet.2007.07.051.

References and notes

1. Rajca, A.; Rajca, S.; Padmakumar, R. *Angew. Chem., Int. Ed. Engl.* **1994**, *33*, 2091–2093.
2. Rajca, A. *Chem. Rev.* **1994**, *94*, 871–893.
3. Rajca, A. *Chem.—Eur. J.* **2002**, *8*, 4834–4841.
4. Rajca, A. *Adv. Phys. Org. Chem.* **2005**, *40*, 153–199.
5. Dougherty, D. A. *Acc. Chem. Res.* **1991**, *24*, 88–94.
6. Iwamura, H.; Koga, N. *Acc. Chem. Res.* **1993**, *26*, 346–351.
7. Borden, W. T.; Iwamura, H.; Berson, J. A. *Acc. Chem. Res.* **1994**, *27*, 109–116.
8. Fang, S.; Lee, M.-S.; Hrovat, D. A.; Borden, W. A. *J. Am. Chem. Soc.* **1995**, *117*, 6727–6731.
9. Rajca, A.; Rajca, S. *J. Chem. Soc., Perkin Trans. 2* **1998**, 1077–1082.
10. *Magnetic Properties of Organic Materials*; Lahti, P. M., Ed.; Marcel Dekker: New York, NY, 1999; pp 1–713.
11. *Molecular Magnetism*; Itoh, K., Kinoshita, M., Eds.; Gordon and Breach: Amsterdam, 2000; pp 1–337.
12. Rajca, A.; Rajca, S.; Desai, S. R. *J. Am. Chem. Soc.* **1995**, *117*, 806–816.
13. Rajca, A.; Lu, K.; Rajca, S. *J. Am. Chem. Soc.* **1997**, *119*, 10335–10345.
14. Rajca, A.; Wongsriratanakul, J.; Rajca, S. *J. Am. Chem. Soc.* **1997**, *119*, 11674–11686.
15. Rajca, A.; Rajca, S.; Wongsriratanakul, J. *J. Am. Chem. Soc.* **1999**, *121*, 6308–6309.
16. Rajca, A.; Wongsriratanakul, J.; Rajca, S. *Science* **2001**, *294*, 1503–1505.
17. Rajca, A.; Wongsriratanakul, J.; Rajca, S. *J. Am. Chem. Soc.* **2004**, *126*, 6608–6626.
18. Rajca, S.; Rajca, A.; Wongsriratanakul, J.; Butler, P.; Choi, S. *J. Am. Chem. Soc.* **2004**, *126*, 6972–6986.
19. Rajca, A.; Wongsriratanakul, J.; Rajca, S.; Cerny, R. L. *Chem.—Eur. J.* **2004**, *10*, 3144–3157.

20. Ulrich, G.; Turek, P.; Ziessel, R. *Tetrahedron Lett.* **1996**, *37*, 8755–8758.
21. (a) Wang, Q.; Li, Y.; Wu, G. *Chem. Commun.* **2002**, 1268–1269; (b) Sato, K.; Sawai, T.; Shiomi, D.; Takui, T.; Wang, Q.; Wang, J. S.; Li, Y.; Wu, G. S. *Synth. Met.* **2003**, 1197–1198.
22. Kröck, L.; Shivanyuk, A.; Goodin, D. B.; Rebek, J., Jr. *Chem. Commun.* **2004**, 272–273.
23. Rajca, A.; Pink, M.; Rojsajjakul, T.; Lu, K.; Wang, H.; Rajca, S. *J. Am. Chem. Soc.* **2003**, *125*, 8534–8538.
24. Rajca, A.; Mukherjee, S.; Pink, M.; Rajca, S. *J. Am. Chem. Soc.* **2006**, *118*, 13497–13507.
25. Sato, H.; Kathirvelu, V.; Spagnol, G.; Rajca, S.; Rajca, A.; Eaton, S. S.; Eaton, G. R.; *J. Phys. Chem.,* submitted for publication.
26. Winalski, C. S.; Shortkroff, S.; Mulkern, R. V.; Schneider, E.; Rosen, G. M. *Magn. Reson. Med.* **2002**, *48*, 965–972.
27. Lurie, D. J.; Maeder, K. *Adv. Drug Delivery Rev.* **2005**, *57*, 1171–1190.
28. Li, H.; He, G.; Deng, Y.; Kuppusamy, P.; Zweier, J. L. *Magn. Reson. Med.* **2006**, *55*, 669–675.
29. Matsumoto, K.; Hyodo, F.; Matsumoto, A.; Koretsky, A. P.; Sowers, A. L.; Mitchell, J. B.; Krishna, M. C. *Clin. Cancer Res.* **2006**, *12*, 2455–2462.
30. Spagnol, G.; Shiraishi, K.; Rajca, S.; Rajca, A. *Chem. Commun.* **2005**, 5047–5049.
31. Ullman, E. F.; Osiecki, J. H.; Boocock, D. G. B.; Darcy, R. *J. Am. Chem. Soc.* **1972**, *94*, 7049–7059.
32. Kopf, P. W.; Kreilick, R. W.; Boocock, D. G. B.; Ullman, E. F. *J. Am. Chem. Soc.* **1970**, *92*, 4531–4535.
33. (a) Davis, M. S.; Morokuma, K.; Kreilick, R. W. *J. Am. Chem. Soc.* **1972**, *94*, 5588–5592; (b) Selected ^{1}H-hyperfine splittings from ^{1}H NMR spectra of phenyl nitronyl nitroxide: *a*H(*para*)=+0.0382 mT and *a*H(*ortho*)=+0.0446 mT.
34. (a) Forrester, A. R.; Hepburn, S. P.; McConnachie, G. *J. Chem. Soc., Perkin Trans. 1* **1974**, 2213–2219; (b) Selected ^{1}H-hyperfine splittings in nitroxides: *a*H(*para*)=0.20 mT in phenyl-*tert*-butylnitroxide and *a*H(*ortho*)=0.24 mT in 3,5-dimethyl-4-methoxyphenyl-*tert*-butylnitroxide.
35. Izuoka, A.; Fukada, M.; Sugawara, T. *Mol. Cryst. Liq. Cryst.* **1993**, *232*, 103–108.
36. Catala, L.; Moigne, J. L.; Kyritsakas, N.; Rey, P.; Novoa, J. J.; Turek, P. *Chem.—Eur. J.* **2001**, *7*, 2466–2480.
37. Verboom, W.; Datta, S.; Reinhoudt, D. N. *J. Org. Chem.* **1992**, *57*, 5394–5398.
38. Tetraaldehyde **4** was previously prepared in 66% yield by the $TiCl_4$-catalyzed formylation with 1,1-dichlorodimethyl ether: Maulucci, N.; De Riccardis, F.; Botta, C. B.; Casapullo, A.; Cressina, E.; Fregonese, M.; Tecilla, P.; Izzo, I. *Chem. Commun.* **2005**, 1354–1356.
39. Shimono, S.; Tamura, R.; Ikuma, N.; Takimoto, T.; Kawame, N.; Tamada, O.; Sakai, N.; Matsuura, H.; Yamauchi, J. *J. Org. Chem.* **2004**, *69*, 475–481.
40. Crystal data for nitronyl nitroxide tetraradical **1**·2.25 C_6H_6·0.25 H_2O: blue block, 0.20×0.15×0.12 mm, $C_{81.50}H_{106}N_8O_{16.25}$, M=1457.74, monoclinic, a=19.576(3) Å, b=31.283(5) Å, c=27.078(4) Å, β=103.362(16)°, V=16,133(4) Å^3, T=130(2) K, space group $P2_1/n$, Z=8, ρ_{calcd}=1.200 Mg m^{-3}, μ=0.084 mm^{-1}, $2\theta_{max}$=45.06, Mo Kα (λ=0.71073). A total of 143,076 reflections were measured, of which 28,452 were independent (R_{int}=0.0777). Final residuals were R=0.1219 and $wR2$=0.3298 (for 16,449 observed reflections with $I>2\sigma(I)$, 1776 parameters, 210 restraints) with GOF=2.155 and largest residual peak 1.207 eÅ^{-3} and hole −0.970 eÅ^{-3}. Crystallographic data (excluding structure factors) for the structure reported in this paper have been deposited with the Cambridge Crystallographic Data Centre as supplementary publication no. CCDC-646077.
41. (a) The C···C distances in Å between co-facial ONCNO groups in tetraradical **1**: C29A···C49A=6.680(7), C39A···C59A=6.893(7), C29B···C49B=7.132(7), and C39B···C59B=6.961(8). These C···C distances are relatively accurate, as they are not affected by any of the disorders, including disorders in side chains and in solvent molecules, as well as the rotational disorder of imidazoline rings; (b) The C···C distances in Å between co-facial ONCNO groups in diradical **2**: C32a···C45a=7.73(3) and C32b···C45b=7.70(3); (c) The (C1–C6)–(C15–C20) and (C8–C13)–(C22–C27) dihedral angles between calculated least-squares planes of the co-facial benzene rings in **1**, **2**, and the corresponding nitroxide tetraradical and diradical are as follows: in **1**, 19.74(9)°, 25.45(22)°, 22.87(12)°, 24.05(22)°; in **2**, 36.2(5)°, 38.9(9)°, 36.7(9)°, 36.3(9)°; in nitroxide tetraradical, 3.62(7)°, 2.85(7)°; in nitroxide diradical, 3.38(19)°, 13.96(17)°, 8.42(9)°, 13.80(18)°.
42. Sharp, R. R. *Nucl. Magn. Reson.* **2005**, *34*, 553–596.
43. (a) Evans, D. F. *J. Chem. Soc.* **1959**, 2003–2005; (b) Live, D. H.; Chan, S. I. *Anal. Chem.* **1970**, *42*, 791–792.
44. Two types of protons (AB or AX spin system) are expected for the methylene groups of the macrocycle in diradical **2**. An AB spin system is observed for the corresponding protons in bis(1,3-dihydroimidazolidine) 7 in DMSO-d_6 at room temperature.
45. The numerical fits with two components, tetraradical and triradical for **1**, and diradical and monoradical for **2**, suggest 99+% content of tetraradical and diradical, respectively.
46. 2-(4′-Hydroxyphenyl)-4,4,5,5-tetramethylimidazoline-1-oxyl-3-oxide and related nitronyl nitroxide radicals, see: Ref. 31.
47. In the point-dipole approximation, $|D/hc|$ is related to $1/r^3$, where r is the radical–radical distance.
48. Very small value of mean-field parameter, $\theta \approx -0.1$ K, is also obtained for 5 mM **2** in chloroform.
49. Rajca, A.; Rajca, S.; Wongsriratanakul, J. *Chem. Commun.* **2000**, 1021–1022.
50. Frank, N. L.; Clérac, R.; Sutter, J.-P.; Daro, N.; Kahn, O.; Coulon, C.; Green, M. T.; Golhen, S.; Ouahab, L. *J. Am. Chem. Soc.* **2000**, *122*, 2053–2061.
51. In addition to intermolecular radical–radical O···O distances of 4.5–6.1 Å, network of short intermolecular radical–radical O···C distances may be identified. For example, the O1–C6(*meta*) contacts at 3.442 Å are between aryl nitronyl nitroxide moieties in the adjacent spiroconjugated diradical molecules, thus effectively forming dimers, i.e., antiferromagnetically coupled pairs of S=1/2 spins. The presence of two O1–C6(*meta*) contacts per pair, which may be viewed as two parallel exchange coupling pathways, will further amplify the strength of the antiferromagnetic coupling (Ref. 49).
52. Microwave saturation may have a significant effect when $|\Delta m_s|$=1 transitions are used for the intensity versus $1/T$ plots near the liquid helium temperature range. Similar artefacts, due to saturation, are likely for very weak $|\Delta m_s|$=2 transitions in diradicals with small values of $|D/hc|$.
53. (a) Rajca, A.; Rajca, S. *J. Am. Chem. Soc.* **1996**, *118*, 8121–8126; (b) Rajca, A.; Lu, K.; Rajca, S.; Ross, C. R., II. *Chem. Commun.* **1999**, 1249–1250.
54. Suffert, J. *J. Org. Chem.* **1989**, *54*, 509–510.
55. Perrin, D. D.; Armarego, W. L. F. *Purification of Laboratory Chemicals*, 3rd ed.; Pergamon: Oxford, 1988; p 365.
56. Carlin, R. L. *Magnetochemistry*; Springer: Berlin, 1986; pp 2–4.